Journal of
Synchrotron Radiation

ISSN 0909-0495

Received 4 February 2009
Accepted 27 April 2009

Surface-sensitive reflection-mode EXAFS from layered sample systems: the influence of surface and interface roughness

P. Keil[a] and D. Lützenkirchen-Hecht[b]*

[a]Department of Interface Chemistry and Surface Engineering, Max-Planck Institut für Eisenforschung GmbH, Max-Planck-Strasse 1, 40237 Düsseldorf, Germany, and [b]Fachbereich C, Physik, Bergische Universität Wuppertal, Gaussstrasse 20, 42097 Wuppertal, Germany.
E-mail: dirklh@uni-wuppertal.de

The calculation of reflection-mode grazing-incidence X-ray absorption spectra from single surfaces and (multi-)layered systems is studied here. In particular, the influence of the surface and interface roughness was investigated in detail. Simulations of grazing-incidence reflection-mode EXAFS spectra using a simple Fresnel theory neglecting any effect of roughness are compared with the Névot–Croce model and the elaborated distorted-wave Born approximation which both include surface and interface roughness. Data are presented for clean gold surfaces, where the strong influence of the surface roughness on the resulting spectra is demonstrated. Furthermore, in the case of layered systems, the influence of both the outer (air or vacuum side) surface roughness and the inner interface roughness on the reflection-mode EXAFS spectra is evaluated. The practical consequences of the observed correlations are discussed, and a quantitative data analysis of a copper sample that was oxidized in ambient air for several months is shown, including the evaluation of specular reflectivity profiles at fixed energy.

Keywords: EXAFS; XANES; reflection mode; grazing incidence; surface roughness; DWBA; copper; oxidation; thin films.

1. Introduction

Grazing-incidence reflection-mode X-ray absorption spectroscopy is a valuable method for obtaining structural information about the near surface region surfaces and thin films, and has proven to be useful for many different research areas such as oxidation by gases and liquids (Bosio *et al.*, 1988; Cortes *et al.*, 1990; Borthen & Strehblow, 1993; Gibson & Crabb, 1995; Hecht *et al.*, 1996), corrosion (Lützenkirchen-Hecht & Frahm, 2005), thin film growth (Charnock *et al.*, 1995; d'Acapito *et al.*, 2002, 2004; Lützenkirchen-Hecht & Frahm, 2006), materials synthesis (Cheong *et al.*, 2001), battery charge and discharge investigations (Lützenkirchen-Hecht *et al.*, 2003; Wagemaker *et al.*, 2004) *etc*. Grazing-incidence X-ray absorption spectroscopy detection techniques currently also include total electron yield (Zheng *et al.*, 1997), fluorescence (Heald *et al.*, 1988), diffusely scattered light (Keil *et al.*, 2005*a*) and the intensity of Bragg rods (Grenier *et al.*, 2001; Luo *et al.*, 2001). Reflectivity XAS data recorded in the vicinity of an absorption edge exhibits a fine structure similar to EXAFS oscillations. However, in comparison with conventional transmission- or fluorescence-mode EXAFS, both the real part $\delta(E)$ and imaginary part $\beta(E)$ of the complex refractive index $n(E) = 1 - \delta(E) - i\beta(E)$ contribute to the reflectivity fine structure depending on the actual grazing angle and the photon energy E. Nevertheless, in the past, short-range-order structural information about surfaces and thin films was derived from reflection-mode EXAFS using the Fresnel theory. In the case of homogeneous samples or thin films with a film thickness larger than the penetration depth of the X-rays into the film, the absorption coefficient can be directly extracted from reflection-mode XAS data by means of a Kramers–Kronig transform, and a conventional EXAFS data analysis yielding coordination numbers, distances and the local disorder around the atom of interest is possible (see, for example, Martens & Rabe, 1980; Borthen & Strehblow, 1995; Lützenkirchen-Hecht & Frahm, 2001; Benzi *et al.*, 2008). However, such an extraction is in general not possible for thin film sample systems with layer thicknesses smaller than the X-ray penetration depth, or in the case of an inhomogeneous distribution of the X-ray absorbing atom within the sample. In those situations the experimental reflection-mode XAS data have to be compared with (*ab initio*) model calculations assuming the presence of certain structures and thicknesses of

the involved surface layers (see, for example, Hecht *et al.*, 1996; Borthen & Strehblow, 1997; Lützenkirchen-Hecht & Frahm, 2006; Benzi *et al.*, 2008). Nevertheless, a variation of the grazing angle allows a depth profiling of the materials under investigation similar to X-ray photoelectron spectroscopy (XPS). Compared with XPS, however, there is no need for ultrahigh-vacuum conditions, *i.e.* solid–liquid interfaces or samples in a reactive gas environment can easily be studied under *in situ* conditions including time-resolved experiments also (Cortes *et al.*, 1990; Gibson & Crabb, 1995; Hecht, Borthen & Strehblow, 1996; Hecht, Frahm & Strehblow, 1996; Cheong *et al.*, 2001; Lützenkirchen-Hecht & Frahm, 2005). However, any real surface/interface is generally afflicted with a variety of surface inhomogeneities such as surface roughness and lateral correlations, and the X-ray reflectivity is affected accordingly. In recent years the understanding of X-ray scattering from roughened single surfaces, multilayers and their interfaces has advanced rather far, and it was shown that the adequate treatment of roughness is a very important part of the calculation of the scattered intensities (Névot & Croce, 1980; Sinha *et al.*, 1988; Hóly & Baumbach, 1994; de Boer & Leenaers, 1996; Tolan, 1999). If only vertical roughness features are considered, only one single roughness parameter is required for each surface/interface. Usually the r.m.s.-roughness σ is used as roughness parameter and in this case the X-ray reflectivity has been formulated a long time ago by extending the Fresnel theory (Parratt, 1954; Névot & Croce, 1980; Sinha *et al.*, 1988). While the application of the Fresnel theory is restricted to calculations of specular reflectivities, more sophisticated calculation schemes such as the distorted-wave Born approximation (DWBA) also allow off-specular reflectivities to be described quantitatively (Sinha *et al.*, 1988; Hóly & Baumbach, 1994; Tolan, 1999). For this purpose, a complete description of the roughness including lateral roughness features is required. The morphology of surfaces and interfaces which exhibit self-affine roughness can be described using height–height correlation functions like $C(\mathbf{R}) = \sigma^2 \exp[(\mathbf{R}/\xi)^{2h}]$, where $\mathbf{R}$ represents the lateral position in the surface plane (Sinha *et al.*, 1988). Thus, a set of three parameters, namely the r.m.s. roughness σ, the lateral correlation length ξ and the Hurst parameter h, is sufficient for the description and characterization of each surface/interface. However, it has to be mentioned that for liquids and interfaces with logarithmic height–height correlation functions more complex models and further parameters have to be used (see, for example, Palasantzas, 1993). While intense calculations and many successful experiments have been performed for specular and non-specular X-ray scattering at fixed photon energies, and thus the influence of the different lateral and vertical roughness features in multilayered samples are well understood, only few studies have been conducted with regard to the influence of roughness on grazing-incidence X-ray absorption spectroscopy, and more specifically on reflection-mode XAS (Borthen & Strehblow, 1997). To our best knowledge, no systematic investigations have been performed so far, and the existing publications show contradictory results. For example, a systematic decrease of the Fourier-transform amplitudes with increasing roughness was found in a study by Borthen & Strehblow (1997), while the opposite was the conclusion of a more recent publication (Keil *et al.*, 2005*b*). Most of the publications up to now have just neglected all roughness effects in the data analysis (*e.g.* Hecht, Borthen & Strehblow, 1996; Hecht, Frahm & Strehblow, 1996; d'Acapito *et al.*, 2002; Cheong *et al.*, 2001; Lützenkirchen-Hecht *et al.*, 2003; Jiang *et al.*, 1991; Jiang & Crozier, 1997; Luo *et al.*, 2001). Such an approach seems to be reasonable for diluted sample systems, *i.e.* samples where the reflectivity is determined by the matrix only and the XAFS under investigation is determined by a very small quantity of an atomic species within the matrix (*e.g.* Jiang *et al.*, 1991; Jiang & Crozier, 1997; d'Acapito *et al.*, 2002). In this case the effect of roughness could be by far less critical as the refraction index of the matrix is without any structure in the energy region considered, and the thickness of the absorbing layer is smaller than the extinction length of the X-rays. However, for non-diluted sample systems a strong influence of the surface roughness of all of the participating layers to the EXAFS signal can directly be expected from the underlying theory. The interface roughness defines the amplitude of the electric field within the sample at a certain depth from the surface, and therefore also the reflectivity as well as all related signals such as the X-ray fluorescence are thus influenced or even determined by the distribution of the material within the penetration depth of the X-rays within the sample (see, for example, de Boer, 1996). It should be noted here that, for a multiple thin-film sample, the electric fields throughout the material can be found by a recursion relation (Parratt, 1954) or alternatively by a matrix formalism (Born & Wolf, 1975; Król *et al.*, 1988).

First systematic studies on the influence of the surface roughness on the resulting EXAFS spectra have recently been performed for simple sample systems, and the Fresnel theory was compared with the Névot–Croce model including surface roughness and the DWBA (Keil *et al.*, 2005*b*). These studies demonstrated the strong influence of the surface roughness on EXAFS amplitudes depending on the actual grazing angle. As a general trend, it was found out that an increasing surface roughness leads to an increase of the intensity of the peaks in the Fourier-transformed data irrespective of the grazing angle (Keil *et al.*, 2005*b*). For a surface roughness below r.m.s. values of $\sim$5–10 Å, only marginal differences to the Fresnel data were observed. This finding explains why it was sufficient to apply the Fresnel reflectivities in many previous studies where films with smooth surfaces were investigated.

Another problem with regard to surface-sensitive XAS experiments is the dramatic change of the X-ray penetration depth in the vicinity of the absorption edge. Thus different depths are probed by the X-rays below, at and above the absorption edge of interest, which complicates especially the analysis of X-ray absorption near-edge spectra measured at grazing incidence. Here we want to investigate in detail the influence of the surface and interface roughness on the resulting reflection-mode XAS spectra. Such an investigation is not only of fundamental interest, owing to its implications

and drawbacks on reflection-mode EXAFS and XANES experiments, data analysis and interpretation.

2. Calculation details

As mentioned in the previous section, both the real (δ) and the imaginary (β) part of the complex refractive index are needed for calculation of the reflectivity as a function of the photon energy. While β was directly derived from measured absorption data by $\beta = \mu\lambda/4\pi$, λ being the X-ray wavelength, δ was calculated from β by means of a Kramers–Kronig transform (Borthen & Strehblow, 1995; Cross *et al.*, 1998; Filatova *et al.*, 1999). Making use of these quantities, energy-dependent reflectivity data were calculated for different model systems, as shown below in more detail. Here especially those systems are of particular interest, where the X-ray absorbing atom is present in several layers which is the case for *e.g.* thin oxide or passive layers on metals or semiconductors, corroded or chemically modified surfaces (*e.g.* Bosio *et al.*, 1988; Cortes *et al.*, 1990; Hecht, Borthen & Strehblow, 1996; Hecht, Frahm & Strehblow, 1996; Lützenkirchen-Hecht *et al.*, 2003; Lützenkirchen-Hecht & Frahm, 2005).

Reflection-mode XAS spectra of layered systems were calculated using a procedure which is given in Fig. 1 as a flow diagram for a layered sample system. In Fig. 1 a thin Au layer on top of a SiO_2 substrate is treated as an example. Similar to the calculation of the angle-dependent reflectivity $R(\Theta)$ at a fixed energy (*i.e.* X-ray reflectometry), the thickness of the surface layer(s) as well as the energy-dependent indices of refraction of both the substrate and the top layer(s) must be known. In the easiest case the latter quantities can be extracted from transmission EXAFS spectra of suited reference compounds. While $\beta(E)$ is correlated with the linear absorption coefficient $\mu(E)$ as already mentioned, $\delta(E)$ can be calculated from $\beta(E)$ by means of a Kramers–Kronig transformation. For a substrate or layers which do not contain the atomic species of the absorption edge under investigation, $\beta(E)$ and $\delta(E)$ do not show any fine structures and these quantities can be directly taken from databases or tabulated values (*e.g.* Henke *et al.*, 1993). With these energy-dependent complex indices of refraction $n(E)$ of each sublayer and the substrate, the reflectivity spectra were obtained as energy-dependent reflectivities $R(E,\Theta)$ similar to the calculation of the reflectivity in X-ray reflectometry. For the latter step we have applied several different calculation schemes including the simple Fresnel reflectivity for smooth surfaces according to Parratt (1954). Roughness is accounted for by including roughness features *via* the addition of the Névot–Croce factor to the reflection and transmission Fresnel coefficients for each layer according to the schemes introduced by Névot & Croce (1980). Alternatively, the DWBA is also applied, making use of the approach of Sinha *et al.* (1988) for single interfaces, while for multilayered systems the procedure described by Hóly & Baumbach (1994) is employed. The calculation procedures are described in detail within the corresponding references and are adapted one by one for the calculation of the reflection-mode EXAFS spectra shown here.

Although the calculation of the X-ray reflectivity based on the Parratt formalism including roughness features (*i.e.* using the Névot–Croce model) is a well established procedure which works well in most cases, severe limitations occur if the roughness of thin films is similar to the film thickness, like in the case of very thin passive oxide layers on metals or semiconductor surfaces. In the case of the Parratt formalism, the interfaces of the layer stack are usually treated independently. Thus, the density profile $\rho(z)$ obtained by the assumption of independent interfaces is no longer continuous if the roughness at the interfaces is similar to the layer thickness itself. Nevertheless, it is still possible to apply the Parratt formalism for the calculation of the reflectivity making use of arbitrary density profiles as shown, for example, by Tolan (1999). However, the corrections introduced to the Parratt formalism are significant only for incidence angles significantly larger than the critical angle of total reflection Θ_c, implying that the Parratt theory is still applicable for grazing angles in the vicinity of the critical angle and below (*e.g.* Tolan, 1999, chapter 2.4). It is important in this context that reflection-mode XAS measurements are usually performed in the latter angular range, and thus, from a technical point of view, the use of the Névot–Croce model is still justified for the calculation of reflection-mode XAS spectra even for those sample systems where the roughness at the interfaces is similar to the layer thickness.

Owing to the calculation procedure, these simulated reflectivity spectra $R(E,\Theta)$ contain the near-range order structural information of the chosen model compounds, either by a direct input of structural parameters and an *ab initio* calculation of the refractive index (Lützenkirchen-Hecht & Frahm, 2006; Benzi *et al.*, 2008) or by using spectra of suited reference compounds (Borthen & Strehblow, 1997; Lützenkirchen-Hecht *et al.*, 2003). Here we have used high-quality transmission-mode XAS data which were obtained from polycrystalline reference materials (metal foils, oxide powders) at beamlines RÖMO 2 and BW1 at HASYLAB (DESY, Hamburg, Germany) operating with 100–150 mA of 4.45 GeV positrons. While home-made computer-programs were used for the calculation of the reflectivity data, the data reduction was performed using the *Athena* package (Ravel & Newville, 2005) and the *WinXas* software (Ressler, 1998).

It should be mentioned here that the calculation scheme presented in Fig. 1 can also be used for fitting the experimental data. Thus, if the calculated specular X-ray reflectivity profile and the calculated reflection-mode EXAFS are not fitting to the experimental data adequately, new model compounds or different thicknesses of the involved materials have to be used. In addition, a multilayered structure instead of a single surface layer may also be required for the simulations in order to obtain a close fit to the experiments. Alternatively to reference compounds, *ab initio* calculations using software codes like *FEFF* (*e.g.* Ankudinov *et al.*, 1998) can also be used as sources for the EXAFS [$\Delta\beta(E)$ and $\Delta\delta(E)$] and the structureless atomic contributions [$\beta_0(E)$ and $\delta_0(E)$] of such reflectivity spectra. Therefore experimental reflectivity data can be directly fitted to structure models, *i.e.* the determination of

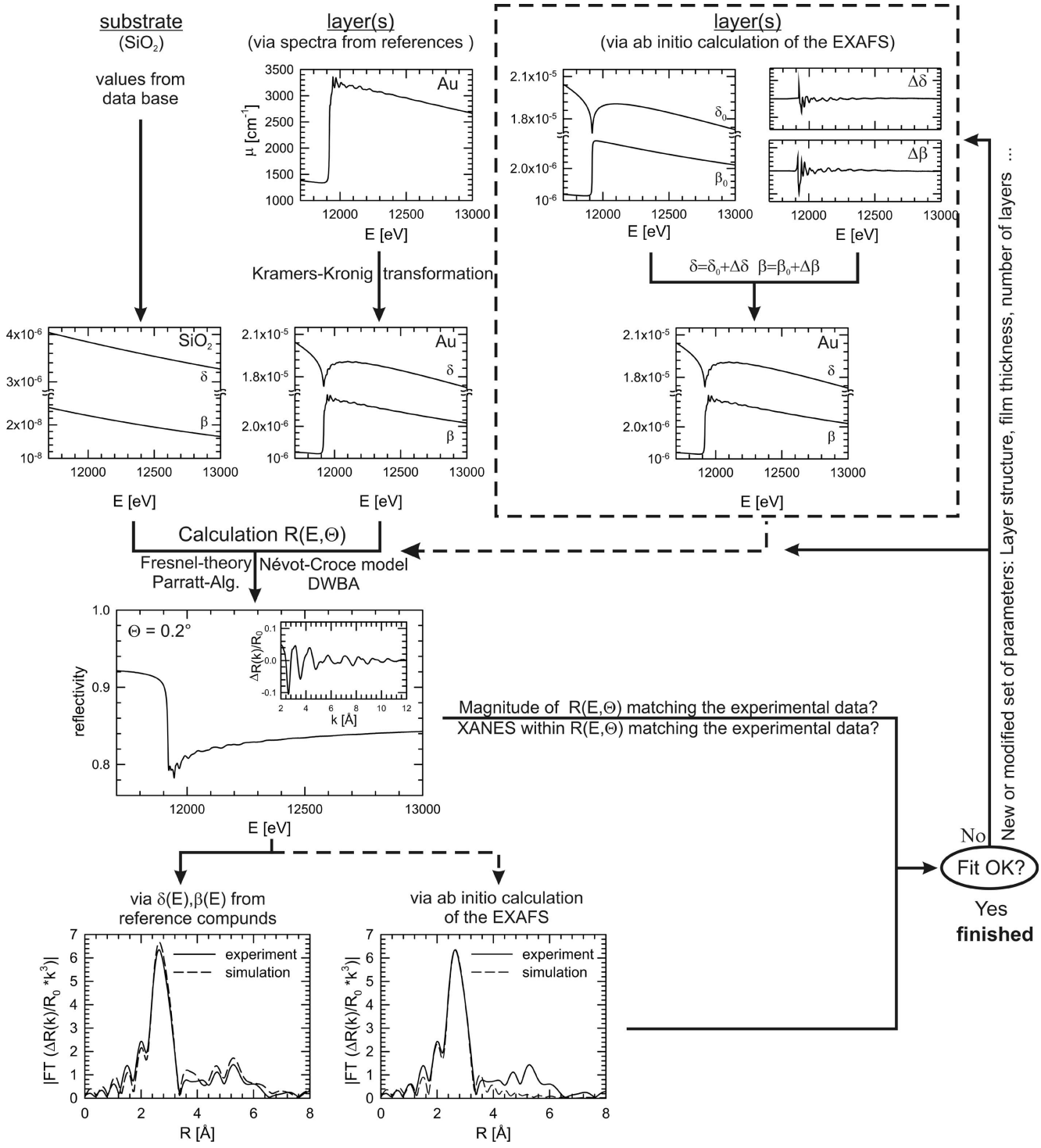

Figure 1
Basic flow chart of the calculation and data analysis scheme of reflection-mode EXAFS spectra, exemplarily shown for the Au L_3-edge EXAFS of a thin gold layer on a SiO_2 substrate. The optical constants $\beta(E)$ and $\delta(E)$ of the Au layer can be either approximated by those of a reference compound (*e.g.* polycrystalline Au) or by *ab initio* calculations.

nearest-neighbour distances, coordination numbers and Debye–Waller factors of surface layers is enabled by adjusting the input parameters of the calculation so that the calculated and measured data show a close fit. A detailed calculation procedure for such kinds of model calculation was recently given by Benzi *et al.* (2008).

3. Results and discussion

In Fig. 2(*a*), calculated reflection-mode EXAFS data at the Au L_3-edge for a pure gold surface are presented for a grazing angle $\Theta = 0.2^\circ$ and different r.m.s. values of the surface roughness making use of the Névot–Croce model. As

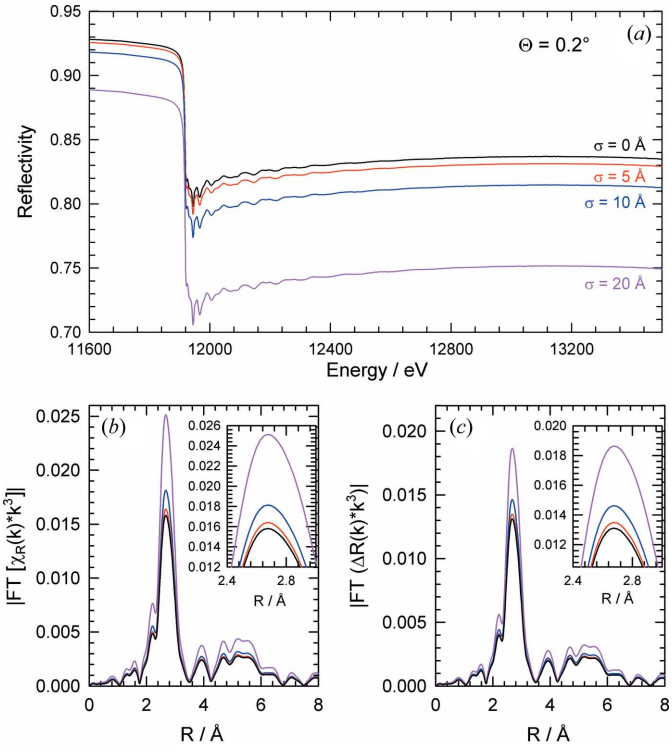

Figure 2
(*a*) Calculated reflection-mode EXAFS spectra for a polycrystalline gold sample at the Au L_3-edge and a grazing angle $\Theta = 0.2°$ for different surface r.m.s. roughness values σ, as indicated. The magnitude of the Fourier transforms (FTs) of the k^3-weighted reflectivity fine structures extracted from these spectra are compared in (*b*) $|\mathrm{FT}[\chi_R(k)k^3]|$ and (*c*) $|\mathrm{FT}[\Delta R(k)k^3]|$, respectively. Black line: Fresnel reflectivity ($\sigma = 0$ Å). Red line: $\sigma = 5$ Å. Blue line: $\sigma = 10$ Å. Purple line: $\sigma = 20$ Å. The insets show the behaviour of the FT in the vicinity of the nearest-neighbour peak in more detail. The data are not corrected for phase shifts; k-range for the FT: 4.5 Å^{-1} < k < 12.5 Å^{-1}.

previously shown, the DWBA gave identical results (see Keil *et al.*, 2005*b*), so we only show one data set here. As expected, the overall reflectivity decreases with increasing surface roughness σ. While only smaller changes can be detected for $\sigma = 5$ Å, a steep reduction of $R(E)$ results for $\sigma = 20$ Å, and it should be noted that the decrease in the energy region above the edge is always larger compared with that in the pre-edge region. This observation directly demonstrates the importance of surface roughness for grazing-incidence X-ray absorption spectroscopy.

In Figs. 2(*b*) and 2(*c*), the Fourier-transformed reflectivity fine-structure data are presented in two different representations as follows. In Fig. 2(*b*), the magnitude of the Fourier transform (FT) of the so-called reduced-reflectivity fine structure

$$\chi_R(k) = \big[R(k) - R_0(k)\big]/R_0(k) = \Delta R(k)/R_0(k), \qquad (1)$$

is presented, where $R(k)$ is the reflectivity of the sample, $R_0(k)$ is the smooth atomic background and k is the photoelectron wavevector, *i.e.* $k = [2m(E - E_0)/\hbar^2]^{1/2}$, where E is the photon energy and E_0 is the energy of the absorption edge under investigation, *i.e.* $E_0 = 11919$ eV in the case of the Au L_3-edge. It should be noted that this representation is most often used in the literature. In the second graph (Fig. 2*c*), the magnitude of the FT of $\Delta R(k)$ is depicted without any further normalizations. Both methods have been used in many papers in the past, but both representations in parallel were scarcely shown. Prior to the calculation of the Fourier transform, the fine structures were k^3-weighted in order to amplify fine-structure contributions at higher k values. As can be seen in both figures, the increase of the surface roughness leads to increasing peak intensities in both Fourier transforms. This is an important observation, because several authors in the past have assumed that, by using the reduced reflectivity $\chi_R(k)$, the effect of surface roughness should cancel out in the data treatment, which is obviously not the case.

Furthermore, by comparing Figs. 2(*b*) and 2(*c*), it can be seen that the increase of the peak maxima with increasing roughness is less pronounced in the case of the FT $[\Delta R(k)k^3]$. For example, for the first-neighbour peak at about 2.7 Å radial distance, the magnitude of FT $[\Delta R(k)k^3]$ has a peak value of about 0.0131 for the Fresnel reflectivity without considering roughness and ~0.0186 for the 20 Å roughness, which corresponds to an increase by about 142%. In the case of the |FT $[\chi_R(k)k^3]$| representation, the increase from ~0.0157 to ~0.0251 amounts to about 160%. Although the effect of roughness is slightly suppressed if pure reflectivities are considered, we can therefore conclude from these calculations that surface roughness has always to be taken into account for a proper data analysis of reflection-mode XAS experiments.

In practical surface analysis studies, it is in some cases only feasible to measure the X-ray absorption near-edge structure (see, for example, Davenport & Sansone, 1995; Schmuki *et al.*, 1996). For (multi-)layered samples, the data analysis in such cases may be extremely difficult because the penetration depth of the X-rays into matter varies dramatically if the photon energy is scanned in the vicinity of an absorption edge while the incidence angle is fixed. This is shown for Cu_2O (cuprite) at the Cu K-edge in Fig. 3 for several different grazing angles. As can be seen, the penetration depth z amounts to only some few nanometres for incidence angles

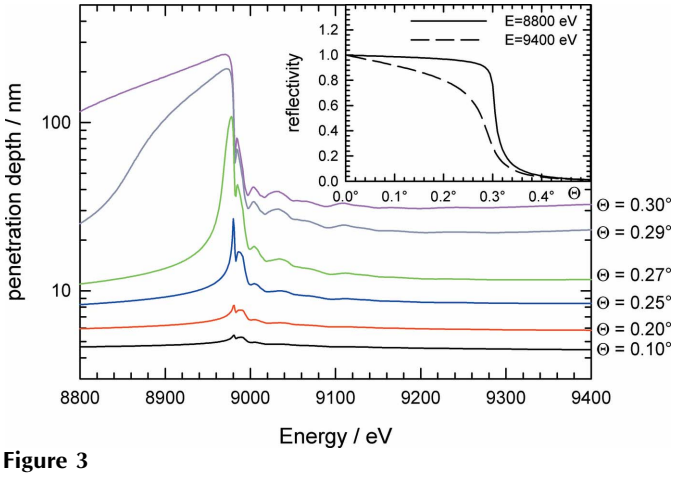

Figure 3
Penetration depth z of X-rays into crystalline Cu_2O in the vicinity of the Cu K-edge for different grazing angles as indicated. The reflectivity at different fixed energies is shown in the inset as indicated.

smaller that the critical angle of total reflection, which amounts to about $\Theta_c = 0.29^\circ$. If Θ is well below Θ_c, z is almost constant throughout the shown energy range. However, if the critical angle is approached for *e.g.* $\Theta = 0.25^\circ$ or $\Theta = 0.27^\circ$, z shows a distinct peaked behaviour in the close vicinity of the absorption edge, with a maximum penetration depth of the order of about 100 nm for $\Theta = 0.27^\circ$, while z amounts to $\sim$11 nm below and above the edge. It is noteworthy to mention here that z is still approximately constant in the EXAFS part of the spectrum for any chosen incidence angle, and thus a depth profiling by EXAFS spectroscopy seems to be feasible as stated by other authors in the past. However, the strong variation of the penetration depth in the edge region makes XANES investigations difficult, for the following reasons. First of all the features in the near-edge spectrum themselves are changing in their relative intensities as a function of the grazing angle even in the case of a semi-infinite sample. In such a case, variations detected in near-edge spectra may be misinterpreted because they are just the consequence of a changed roughness and an accordingly modified X-ray penetration into the sample. Second, and more intriguing, in the case of a layered system the substrate or any underlying material may contribute in different amounts accordingly. One may argue that some of those implications may be overcome by performing the reflection-mode EXAFS scans in such a way that the z-component of the scattering wavevector $q_z = 4\pi \sin\Theta/\lambda$ is kept constant during the scan by a small variation of the incidence angle Θ simultaneously with the photon energy. However, since the penetration depth of the X-rays is mainly determined by the energy dependence of δ and β, the dramatic changes of z at the edge will still be present, even if such a complication to the scattering geometry is added. Furthermore, the changes of q_z in a typical EXAFS scan are usually small. Assuming, for example, an incidence angle of $\Theta = 0.2^\circ$, q_z varies from 0.031 Å^{-1} at 8800 eV in the pre-edge region to $\sim$0.032 Å^{-1} directly at the Cu *K*-edge at 8979 eV, to $\sim$0.033 Å^{-1} at 9400 eV.

We have therefore performed calculations on a model system consisting of a thin layer composed of Cu_2O (crystalline cuprite) on metallic copper, *i.e.* the X-ray absorbing species is present in both the overlayer and the substrate. The layer thickness was set to 3.5 nm, and therefore the whole copper oxide film is penetrated by the X-rays even for incidence angles smaller than Θ_c. The roughness of the outer air–Cu_2O surface and the inner Cu_2O–Cu metal interface were varied systematically. The calculations were performed in the framework of the Névot–Croce model and the results are compiled in Fig. 4. It should be mentioned at this point that calculations of the same Cu_2O–Cu system utilizing the DWBA lead to identical results. As can be seen, the edge jump increases continuously with increasing roughness σ_1 of the outer Cu_2O layer if the interface roughness between the Cu_2O and the Cu metal is set $\sigma_2 = 0$. In addition, the near-edge features, *e.g.* the absorption maximum at 8992 eV, are also increasing with σ_1, which demonstrates the difficulty of a quantitative analysis of near-edge absorption features in the case of rough surfaces. In contrast, for $\sigma_1 = 0$, the edge jump as well as the reflectivity remain almost unaffected if the inner interface roughness σ_2 is increased. Only for $\sigma_2 = 30$ Å does the double-peaked XANES features typical for metallic copper appear at $\sim$8992 eV and 9001 eV. For comparison, we have included a spectrum calculated for a pure metallic Cu sample neglecting roughness. As can be seen, the mentioned structures are characteristic of metallic copper as already stated, and therefore we can conclude that roughening of the inner Cu_2O/Cu interface obviously leads to more pronounced contributions of the underlying metal to the XANES signals, and a quantitative fit of the spectrum would have led to an

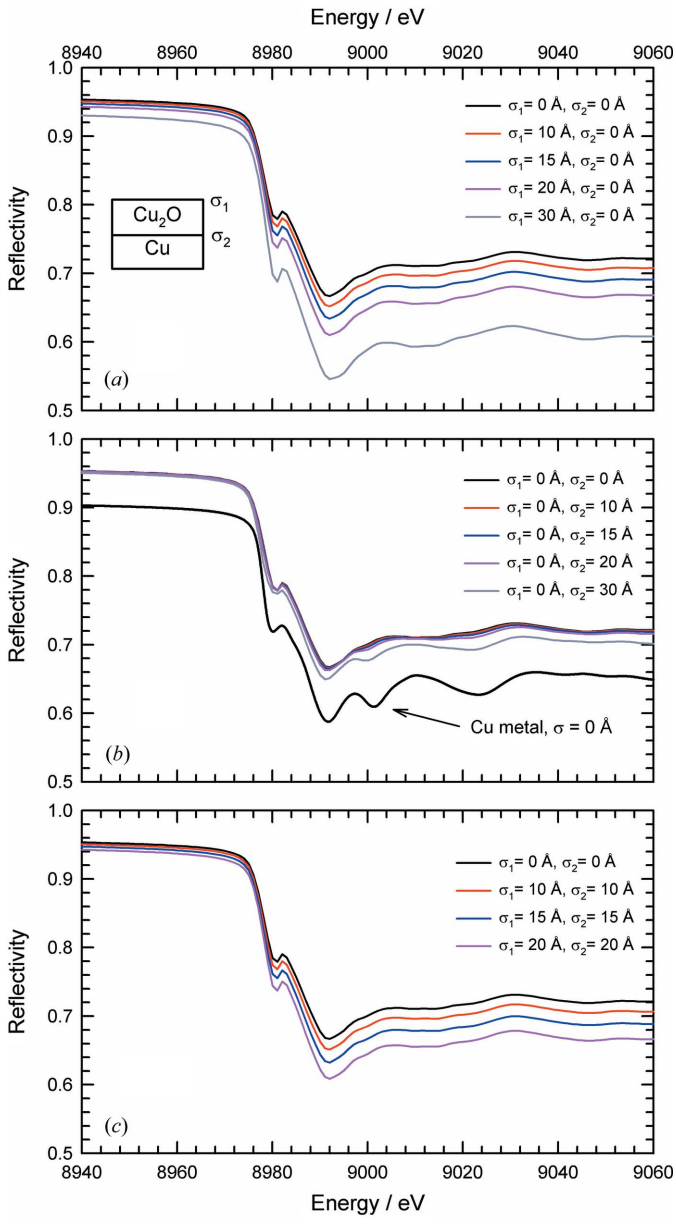

Figure 4
Calculated reflection-mode X-ray absorption near-edge spectra for a layer of 3.5 nm crystalline Cu_2O on a copper metal substrate [as shown schematically in the inset of Fig. 3(*a*)] and a grazing angle $\Theta = 0.2^\circ$ and various different r.m.s. roughness values for the Cu_2O/air surface (σ_1) and the inner Cu_2O/Cu interface (σ_2) as indicated. For comparison, a spectrum of a smooth ($\sigma = 0$ Å) oxide-free Cu metal sample is shown in (*b*); this spectrum is shifted downwards by 0.05 for a better visualization.

overestimation of the metallic content in comparison with the Cu oxide surface layer. On the other hand, owing to the more developed oxidic absorption features which result from the roughening of the outer surface, the Cu_2O contribution or the thickness of the oxide layer would have been overestimated if the influence of surface and interface roughness were neglected. In Fig. 4(*c*), both interfaces are afflicted with a non-vanishing roughness. No clear trend can be found here, but, as those calculations have shown, the interplay between the roughness parameters of both contributing interfaces seems to be essential for the quantitative analysis of reflection-mode X-ray absorption near-edge spectra measured at grazing incidence.

In Fig. 5, results of simulations covering the full EXAFS range (*i.e.* up to ∼700 eV above the Cu *K*-edge) of the same sample system are presented for an incidence angle $\Theta = 0.2^\circ$. Clear signatures of cuprite and copper metal are found in the shown Fourier transforms, which can be expected from the penetration depth of the X-rays of about 6 nm (see Fig. 3). As can be seen in Fig. 5(*a*), an increase in the surface roughness of the outer air–cuprite surface leads to an increase of peak intensity of those peaks which belong to oxide coordinations, most prominently the nearest-neighbour Cu—O peak at about 1.3 Å and the first Cu—Cu coordination in the oxide at 2.8 Å. All the peaks are shifted towards smaller distances because of the phase shifts of the scattered photoelectrons, *i.e.* the true crystallographic distances are 1.826 Å and 2.982 Å for the two oxide shells and 2.556 Å for the first coordination of Cu metal. This peak of the underlying metal at about 2.2 Å radial distance and additional Cu metal peaks between ∼4 Å and 6 Å do not change systematically in intensity when the surface roughness of the outer oxide surface is increased. In contrast, if the roughness of the outer surface is kept identical to zero and the roughness of the inner oxide/metal interface is varied, mostly those coordinations belonging to the metal are affected (Fig. 5*b*). Again, an increasing interface roughness leads to increasing peak intensities. However, the peaks of the oxide, especially the Cu—Cu coordination of the oxide at ∼2.8 Å radial distance, are also slightly affected; however, their intensities are decreasing with increasing interface roughness. In Figs. 5(*c*) and 5(*d*), both the roughness at the inner and the outer interfaces were afflicted with a non-zero roughness. As can be seen in Fig. 5(*c*), identical values of both roughness parameters seem to have only a small influence on the calculated reflection-mode EXAFS spectra, as the intensities of all peaks are only increased by about 3–5% for 10 Å and by about 7–15% for 15 Å surface/interface roughness. The last simulation clearly shows that one has to be very careful when reflection-mode XAS data are only available for a single grazing angle. Here the roughness parameter of the outer surface is set constant to $\sigma_1 = 10$ Å, and the influence of σ_2 on the resulting EXAFS spectra is demonstrated. As can be seen here, the increase of σ_2 leads to a steep decrease in intensity of all the oxide coordinations, while that of the Cu—Cu of the metal is strongly enhanced. However, the damping in the oxide intensity is not as developed as the increase of the metal peaks. Although the effects shown in Figs. 4 and 5 are quite

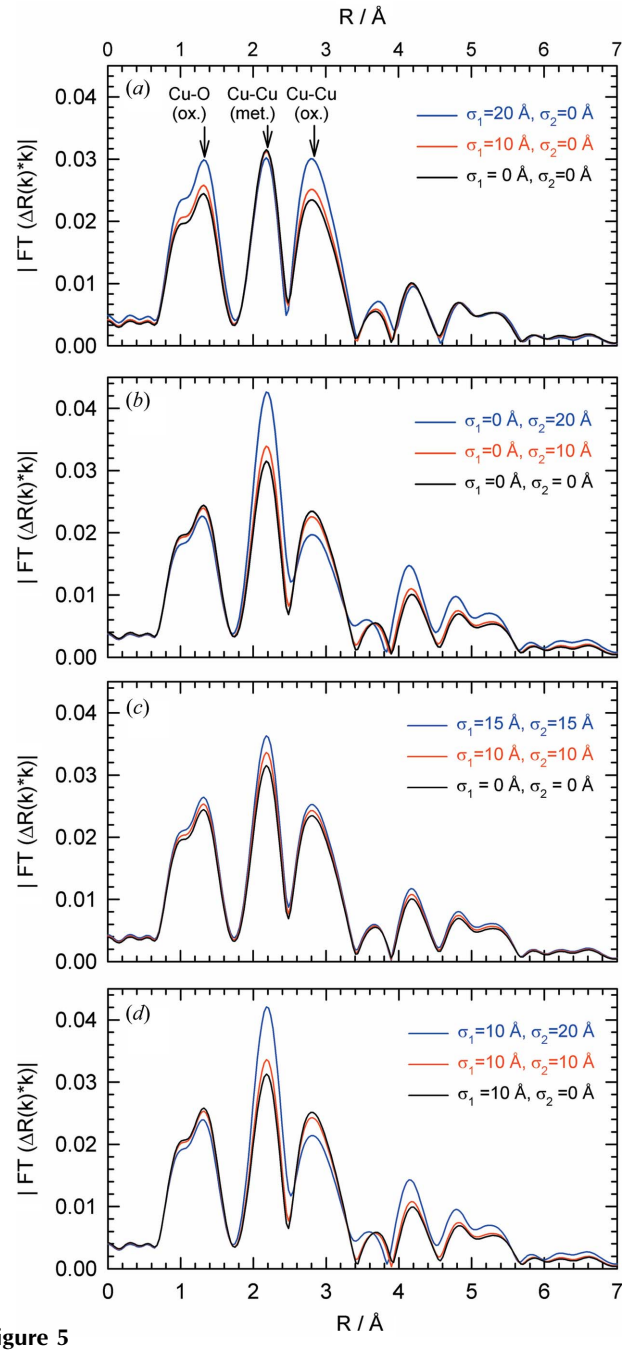

Figure 5
Magnitude of the Fourier transforms (not phase-shift corrected) of the *k*-weighted reflectivity fine structures for calculated reflection-mode EXAFS data ($\Theta = 0.2^\circ$) from a 3.5 nm thin Cu_2O layer on a copper metal substrate for different surface (σ_1) and interface (σ_2) r.m.s. roughness values, as indicated. The calculations were performed in the framework of the DWBA assuming a correlation length of $\xi = 50$ nm and a Hurst parameter $h = 1$ for both interfaces. Calculations within the Névot–Croce model lead to the same FTs. The peaks at $R_1 \simeq 1.3$ Å and $R_3 \simeq 2.8$ Å are related to the first Cu—O and Cu—Cu coordination shells of the copper oxide; the maximum at $R_2 \simeq 2.2$ Å belongs to the first Cu—Cu coordination of metallic copper. (*k*-range for the FTs: 1.75 Å^{-1} < *k* < 11.75 Å^{-1}.)

intriguing, it is difficult to provide an illustrative model for these observations because, statistically, most of the scattering processes of the photoelectron waves which are responsible for the EXAFS will occur well away from the surface.

However, as the roughness determines or at least strongly influences the decay of the electric field strength with depth in the sample, it is on the other hand clear that regions in different depths of the sample contribute to the reflectivity signal with varying intensity, and the total reflectivity signal is a weighted sum over all these different contributions (Parratt, 1954; Born & Wolf, 1975; Król *et al.*, 1988). If a thin film on a substrate is assumed, the variations of the surface and interface roughness thereby change the distribution of the X-ray absorbing species within the penetration depth of the X-rays (de Boer, 1996), and in the detected reflectivity EXAFS signal the respective contributions are affected accordingly.

More data are compiled in Figs. 6(*a*)–6(*c*), where the peak intensities of the mentioned oxide (R_1, R_3) and metal (R_2) peaks are plotted as a function of the roughness parameters σ_1 and σ_2. Peaks R_1 and R_3 obviously show a similar, but not identical, behaviour whereas peak R_2 reveals a directly opposed trend.

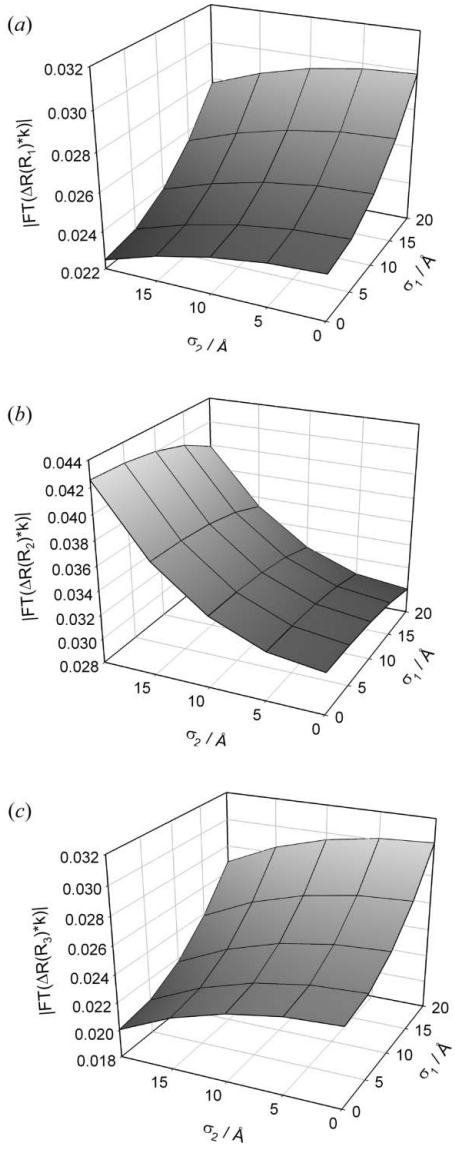

Figure 6
Systematic variations of the peaks belonging to the first Cu—O shell of the oxide at R_1 (*a*), the first Cu—Cu shell of metallic copper at R_2 (*b*), and the Cu—Cu shell of the oxide at R_3 (*c*) as a function of the surface and interface r.m.s. roughness parameters σ_1 and σ_2 according to a simulation assuming a 3.5 nm-thick Cu_2O film on Cu and an incidence angle of $\Theta = 0.2°$.

We can conclude here that the various peaks in the Fourier transforms belonging to species within the layer or to those located in the substrate have a different response to the different roughness parameters in the case of rough surfaces and interfaces, and therefore any quantitative reflection-mode EXAFS data analysis may be directly affected. Moreover, if surface and interface roughness are neglected, data misinterpretations are possible as will be demonstrated by considering our Cu_2O/Cu model system (3.5 nm Cu_2O on Cu) again. Assuming that this thin copper oxide layer is grown homogeneously on a copper metal, it can be assumed that the roughness of both involved interfaces is identical, *i.e.* $\sigma_1 = \sigma_2$. We have chosen a roughness $\sigma_1 = \sigma_2 = 15$ Å which is a reasonable value for a real surface. Let us now consider the three major peaks R_1, R_2 and R_3 separately, *i.e.* the FT was fitted to a theoretical model without accounting for roughness and just matching the value of the peak position and intensity by varying the thickness of the Cu_2O layer in the Fresnel theory using ideally smooth surfaces. As can be seen in Fig. 7, a self-consistent modelling of the 'experimental data' is impossible using the thickness of the oxide as the only fit parameter. While an oxide thickness of only 3.5 nm was used for the rough model sample, the fits disregarding roughness give $d = 4.3$ nm and $d = 3.9$ nm if the first Cu—O at ∼1.3 Å radial distance and the first Cu—Cu peak of the oxide at ∼2.8 Å are optimally fitted. For those two fits, the leading peak of the underlying metal was not reproduced adequately; the simulations gave much too small metal peak amplitudes

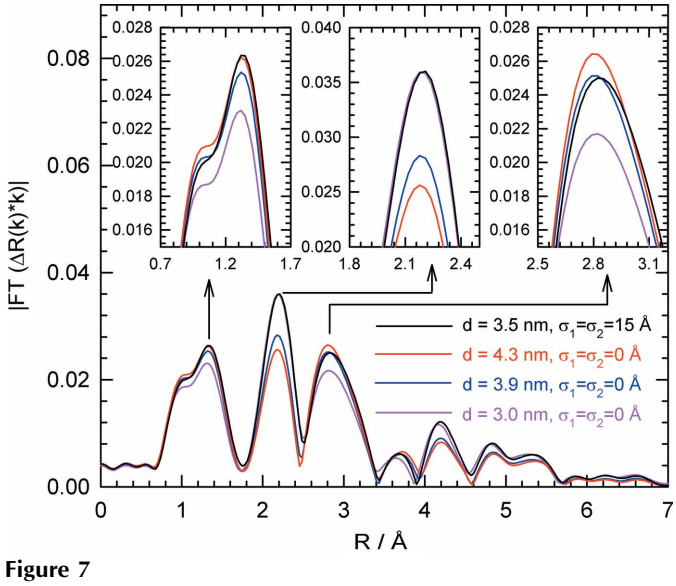

Figure 7
Magnitude of the Fourier transforms of the *k*-weighted reflectivity fine structures calculated for a Cu_2O film of 3.5 nm thickness on a Cu substrate each with 15 Å surface roughness compared with several model systems with different thickness of the Cu_2O layer neglecting any surface and interface roughness, *i.e.* $\sigma_1 = \sigma_2 = 0$ Å. (Incidence angle $\Theta = 0.2°$; the data are not corrected for phase shifts. *k*-range for the FTs: 1.75 $Å^{-1} < k <$ 11.75 $Å^{-1}$.)

in this situation. Even if, for example, the FT is optimally described in the region of the first peak R_1 by the calculation, then the second oxide peak R_3 is overestimated by the calculation and *vice versa*. In contrast, if the Cu—Cu peak of the metal (R_2 at ∼2.2 Å) is well described by a simulation without using any roughness, then an oxide layer thickness of only 3.0 nm results. However, the peaks of the oxide layer are in this case significantly underestimated by about 12% (R_1) and 18% (R_3). In contrast, if R_1 or R_3 are reproduced by the fit to a good approximation, then peak R_2 is underestimated by about 21% up to more than 28%. In contrast to a previous publication where it was stated that any present surface roughness decreases the contributions of surface layers in the Fourier transform (Borthen & Strehblow, 1997), the present investigation has clearly shown that the surface roughness does not have such a simple impact on the reflection-mode EXAFS data, and that the neglect of surface roughness has therefore no easily predictable influence on the obtained results. Moreover, it is also clear that all the different peaks belonging to the layer and the substrate species may not be reproduced by a simulation employing only one single roughness parameter.

In order to demonstrate practical consequences of the observed correlations and dependencies between reflection-mode EXAFS data and the involved layers and materials, we consider experimental data obtained from an oxidized copper specimen in the following. The sample consists of a sputter deposited Cu-metal layer of ∼90 nm thickness on a float glass substrate (Pilkington, Germany), and it was exposed to laboratory air for about nine months prior to the X-ray investigations at the BW1 beamline at HASYLAB (DESY, Hamburg, Germany). Under these environmental conditions, copper is known to form thin passivating oxide films on its surfaces, which prevent the underlying metal from further oxidation or corrosive attack (*e.g.* Barr, 1994; Lenglet *et al.*, 1995; Millet *et al.*, 1995; Apen *et al.*, 1998; Yang *et al.*, 1998). This property is extremely important with regard to the use of Cu in microelectronic circuits *etc.* (Frankenthal, 1990; Koetter *et al.*, 2000). Several different reactions were considered to be involved in the oxide film formation, *i.e.*

$$2\mathrm{Cu} + \mathrm{H_2O} \rightarrow \mathrm{Cu_2O} + \mathrm{H_2},$$
$$\mathrm{Cu} + \mathrm{H_2O} \rightarrow \mathrm{CuO} + \mathrm{H_2},$$
$$\mathrm{Cu} + 2\mathrm{H_2O} \rightarrow \mathrm{Cu(OH)_2} + \mathrm{H_2},$$

although the first process seems to dominate according to Barr (1994) and Apen *et al.* (1998). In Figs. 8 and 9 we present results of reflection-mode EXAFS spectra measured at the Cu *K*-edge for different grazing angles below, at and above the critical angle of total reflection, which amounts to $\Theta_c \simeq 0.29°$, and in Fig. 10 we present a conventional specular X-ray reflectivity profile for a photon energy of 8048 eV (λ = 1.54 Å); here the incidence angle scale was converted to a scattering wavevector q_z scale according to $q_z = 4\pi \sin\Theta/\lambda$.

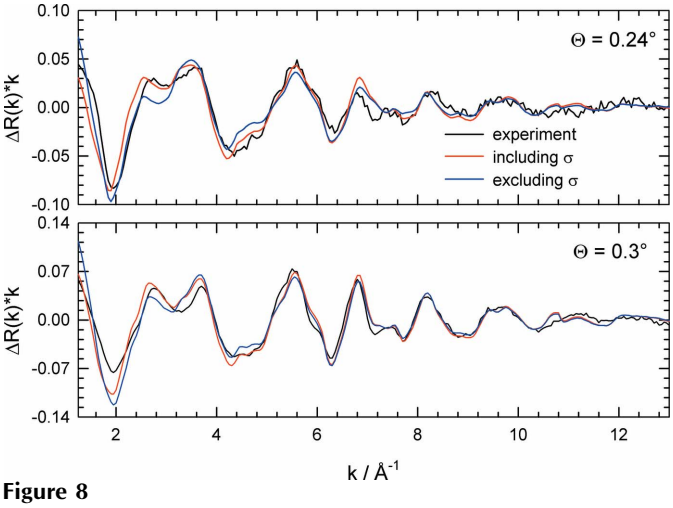

Figure 8
Comparison of the measured reflection-mode Cu *K*-edge EXAFS of an oxidized Cu metal thin film (black line) with calculated data assuming a double-layered oxide structure with d_1(CuO) = 2.0 nm, d_2(Cu_2O) = 3.5 nm and d_3(Cu metal) = 88 nm on a glass substrate. While the first simulation (red line) includes the roughness effects for the different surfaces and interfaces (*i.e.* $\sigma_1 = \sigma_2 = \sigma_3 = 13$ Å for all the interfaces where the oxides are contributing, and $\sigma_4 = 4$ Å for the interface between the smooth glass substrate and the Cu film), any surface roughness is neglected in the second simulation (blue line).

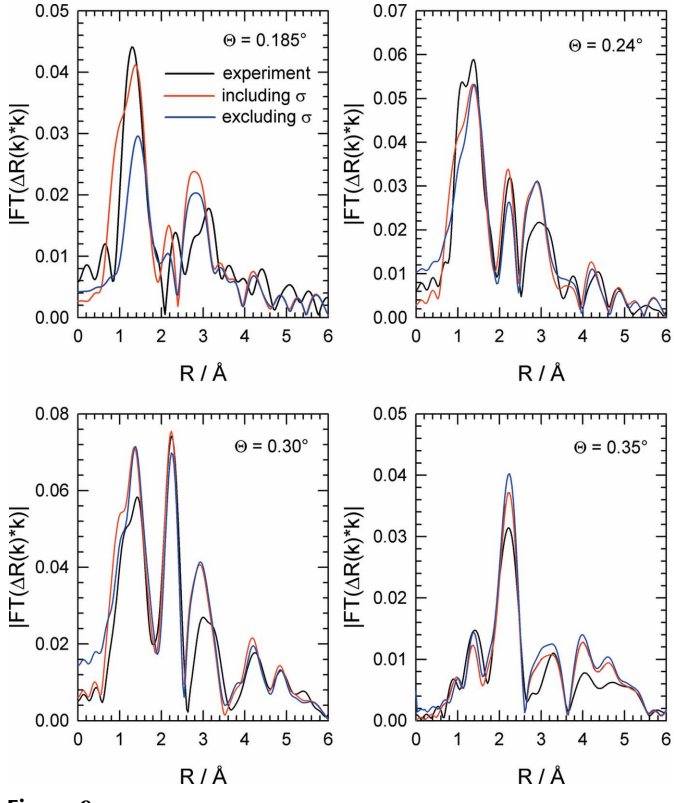

Figure 9
Comparison of the Fourier transforms of measured reflection-mode Cu *K*-edge EXAFS of an oxidized Cu metal thin film (black line) with those of calculated data assuming a double-layered oxide structure with d_1(CuO) = 2.0 nm, d_2(Cu_2O) = 3.5 nm and d_3(Cu metal) = 88 nm on a glass substrate. While the first simulation (red line) includes the roughness effects for the different surfaces and interfaces (*i.e.* $\sigma_1 = \sigma_2 = \sigma_3$ = 13 Å for all the interfaces where the oxides are contributing, and σ_4 = 4 Å for the interface between the smooth glass substrate and the Cu film), any surface roughness is neglected in the second simulation (blue line). (*k*-range for the FTs: 1.75 Å^{-1} < *k* < 11.75 Å^{-1} for Θ = 0.185°; for all other experiments at larger angles, 1.75 Å^{-1} < *k* < 12.75 Å^{-1}.)

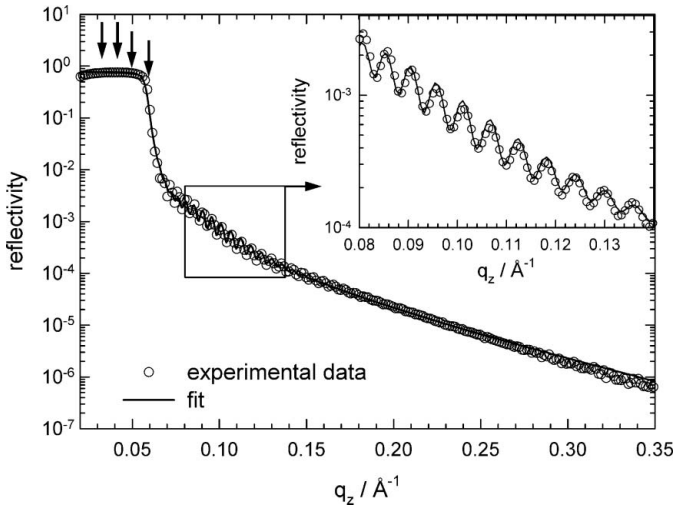

Figure 10
Specular X-ray reflectivity (symbols) and fit (line) for 8048 eV photons (λ = 1.54 Å) of the oxidized Cu metal thin film with the corresponding EXAFS data shown in Figs. 8 and 9. The data refinement was performed by assuming a CuO/Cu_2O double-layered oxide structure on top of the thin copper film. The fit results are: d_1(CuO) = 2.2 nm, d_2(Cu_2O) = 3.2 nm and d_3(Cu metal) = 90.9 nm, ρ_1(CuO) = 6.1 g cm^{-3}, ρ_2(Cu_2O) = 5.7 g cm^{-3} and ρ_3(Cu metal) = 8.4 g cm^{-3}, $\sigma_1 = \sigma_2 = \sigma_3$ = 12 Å and σ_4 = 4 Å, whereas the same value for the roughness was assumed for the data refinement for all the interfaces where the oxides are contributing. The inset displays a magnification of the region well above the critical angle of total reflection to resolve the thickness fringes more clearly. The vertical arrows indicate the maximal q_z values of the reflection-mode EXAFS data shown in Fig. 9 (Θ = 0.185°: 0.029 Å^{-1} < q_z < 0.032 Å^{-1}; Θ = 0.24°: 0.038 Å^{-1} < q_z < 0.041 Å^{-1}; Θ = 0.3°: 0.048 Å^{-1} < q_z < 0.051 Å^{-1}; and Θ = 0.35°: 0.056 Å^{-1} < q_z < 0.06 Å^{-1}.)

Assuming a duplex structure of the oxide with an outer CuO and an inner Cu_2O layer, a quantitative fit of the experimental data was obtained, yielding d_1(CuO) = 2.2 nm, d_2(Cu_2O) = 3.2 nm and d_3(Cu metal) = 90.9 nm, ρ_1(CuO) = 6.1 g cm^{-3}, ρ_2(Cu_2O) = 5.7 g cm^{-3} and ρ_3(Cu metal) = 8.4 g cm^{-3}, $\sigma_1 = \sigma_2 = \sigma_3$ = 12 Å and σ_4 = 4 Å. The high quality of the fit can be seen more clearly in the inset of Fig. 10, where the q_z range between 0.08 Å^{-1} and 0.14 Å^{-1} is shown in a magnified view. One may argue that using only one single roughness parameter for all these different surfaces and interfaces may not be adequate in the present situation. However, previous X-ray reflectivity experiments have shown that thin oxide layers of some few nanometres seem to follow the contour of the underlying metal (You *et al.*, 1992), and thus it seems reasonable to assume that the duplex film has approximately the same surface and interface roughness as the underlying metal, and more specifically also the interfaces within the oxide scale. Furthermore, such a simplification reduces the number of free fit variables considerably, although a variation is in principle possible. The fit quality in addition also supports that this assumption is justified.

We have used these values as a starting point for the fit of the reflection-mode EXAFS data shown in Figs. 8 and 9. The refinement shows that the values for the roughness parameters do not need to be changed, but it finally yields slightly changed thickness values for the contributing layers, *i.e.* a value of d_1 = 2.0 nm for the outer CuO layer, d_2 = 3.5 nm for the inner Cu_2O layer, and d_3 = 87.0 nm for the Cu metal substrate. For comparison, we show a second simulation in which all surface roughness is neglected, *i.e.* $\sigma_1 = \ldots = \sigma_4 = 0$.

First of all, it should be noted at this point that all simulations using only pure Cu_2O-type oxide layer cannot match the experimental data satisfactorily. While the scattering contrast between CuO and Cu_2O is relatively weak in the specular reflectivity profiles because of their similar densities, both compounds reveal significantly different features in their X-ray absorption spectra, and they can thus be separated quite easily. Therefore especially the fitting of our experimental reflection-mode EXAFS data gave clear evidence for the presence of a duplex copper oxide layer with a CuO layer in contact with the oxidizing atmosphere and an inner Cu_2O layer in contact with the metal; such a layering of the oxide was previously observed for the oxidation of copper in alkaline media (Strehblow & Titze, 1980; Lohrengel *et al.*, 1987; Melendres *et al.*, 1998) and more recently also in the case of the native oxide formed on Cu in air (Iijima *et al.*, 2006). According to Iijima *et al.* (2006) the formation of the native oxide layer on top of copper surfaces does not necessarily lead to an amorphous oxide structure. In fact, they have shown that at least the outermost CuO layer is of a polycrystalline nature which motivates the use of polycrystalline reference compounds for the calculation of the reflection-mode EXAFS spectra in this study.

As can be seen in Fig. 8 and even more clearly in Fig. 9, the neglect of surface and interface roughness leads to larger overall differences with the experimental data. Especially for the smallest incidence angle Θ = 0.185°, the amplitude of the Cu—O nearest-neighbour peak at 1.3 Å in the FT cannot at all be reproduced by the simulation, *i.e.* the amplitude is almost 50% too small in comparison with the experimental data. This would suggest a significantly larger film thickness of the oxide layers if only this incidence angle would be considered. However, such an enlarged thickness would at the same time result in significantly smaller metal substrate peak intensities, as with increasing top oxide layer thickness all peaks corresponding to the metal substrate would be reduced in magnitude substantially, even for grazing angles larger than the critical angle of total reflection. The importance of including the surface and interface roughness in the calculation is also reflected within the reflectivity fine structure presented in Fig. 8, where the reflectivity fine structure $\Delta R(k)k$ is shown exemplarily for two different grazing angles. Especially in the range 2 Å^{-1} < k < 5 Å^{-1}, the reflectivity fine-structure oscillations are better reproduced by the model calculations which included roughness, *i.e.* the chosen layer structure and their morphological parameters appear to be suited to describe the experimental situation.

Obviously, in most cases one can find a suitable model that fits to the experimental data well for one selected grazing angle within the framework of the Fresnel theory, simply by adapting the thickness of the contributing metal and/or oxide layers. As shown in Fig. 11 for comparison, the measured data can be fitted reasonably well by using only the Fresnel theory for film thicknesses of d_1(CuO) = 4.5 nm and d_2(Cu_2O) = 4 nm

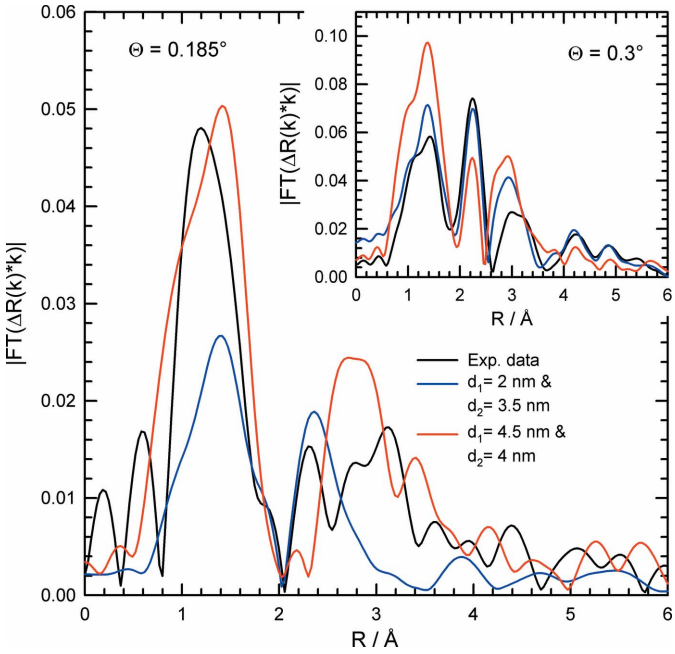

Figure 11
Comparison of the measured reflection-mode Cu *K*-edge EXAFS at a grazing angle of Θ = 0.185° of an oxidized Cu metal thin film with calculated data assuming a double-layered oxide structure with different film thicknesses for the CuO layer (d_1) and the Cu_2O layer (d_2) on top of the copper layer. All the calculations were made within the framework of the Fresnel theory neglecting roughness effects for the different surfaces and interfaces. In the inset, the calculations are compared with the measured data at a grazing angle of Θ = 0.3° (*k*-range for the FTs: 1.75 Å^{-1} < *k* < 11.75 Å^{-1} for Θ = 0.185°, and 1.75 Å^{-1} < *k* < 12.75 Å^{-1} for Θ = 0.30°, respectively.)

at a grazing angle of Θ = 0.185°. However, this data set does not at all fit to the experimental data measured for higher grazing angles, like, for example, for Θ = 0.3° which is shown for comparison in the inset of Fig. 11. In the latter case, the amplitude of the Cu—O nearest-neighbour peak at 1.3 Å as well as the first Cu—Cu coordination of the oxides at ∼2.8 Å radial distance cannot at all be reproduced by the simulation which gives much higher FT amplitudes for these coordinations. Additionally, a native oxide thickness of around 8.5 nm seems to be too large compared with values reported in the literature (see, for example, Iijima *et al.*, 2006). In contrast, thicknesses of d_1(CuO) = 2 nm, d_2(Cu_2O) = 3.5 nm give a reasonable fit for Θ = 0.3°, reproducing both the metal as well as the oxide (first Cu—O shell) peak positions and amplitudes sufficiently. Again, however, such a model is not suited for a satisfactory fit of the experimental data at the smaller grazing angle Θ = 0.185°, where the oxide peaks at ∼1.3 Å and 2.8 Å are much too small in amplitude, while at the same time the amplitude of the Cu—Cu peak of the underlying metal substrate at ∼2.2 Å radial distance is too large.

Thus one important conclusion from the present study is that several different incidence angles below, at and above the critical angle of total reflection must be considered for a meaningful reflection-mode EXAFS data evaluation in general. Furthermore, neglecting surface roughness leads to several smaller deviations between both simulations and the experiment. For example, for incidence angles exactly at the critical angle (*i.e.* Θ = 0.30° in Fig. 9) the metal contributions at 2.2 Å radial distance are underestimated by about 6–7%, while the peak intensity for larger incidence angles shows an antipodal behaviour, *i.e.* the simulation suggests a significantly larger amplitude compared with the experiment and the simulation which includes roughness effects. It has to be stressed that these observations are a proof of the importance and significance of surface and interface roughness for grazing-incidence X-ray absorption spectroscopy.

4. Conclusion and outlook

The influence of surface and interface roughness parameters on reflection-mode EXAFS spectra from layered systems has been investigated in detail. Those situations where the X-ray absorbing element is present in more than one of the layers, or in the layer and the substrate, are especially considered. It can be concluded that surface and interface roughness is an important parameter for any quantitative reflection-mode EXAFS data analysis. Only in the case of smooth surfaces revealing a roughness σ below 10 Å are the changes introduced in the reflection-mode XAFS data of minor importance; however, even in these cases it should be considered whether precise results are expected from the experiments. With increasing surface and interface roughness, an increasing influence of σ on the resulting fine-structure data was found, and a non-consideration of roughness may lead to erroneous results in terms of the coordination numbers or disorder parameters of the respective species, or the thickness of the related layers. In general, thus, for the detailed modelling of experimental reflection-mode EXAFS data a huge number of parameters (bond distances, coordination numbers, disorder parameters, layer thicknesses, roughness parameters *etc.*) may be required (see also Benzi *et al.*, 2008), which in particular may render the practical data analysis rather difficult, even in the case of a rather simple sample system such as the oxidized copper surfaces treated in the present contribution. Anyhow, the number of free parameters can be reduced by assigning the morphological parameters of the layer structure by means of the analysis of the reflectivity at a fixed energy or, even better, by a simultaneous fit of X-ray reflectometry data and the reflection-mode XAFS spectra. It should be noticed that such a procedure has also recently been successfully introduced to magnetic soft X-ray scattering (*e.g.* Tonnerre *et al.*, 2008).

In parallel, however, the results presented here have demonstrated that it is generally required to measure reflection-mode EXAFS data of layered sample systems for several grazing angles below, at and above the critical angle of total reflection, and those data have to be modelled consistently with one single set of parameters. This procedure consolidates the obtained results significantly and thus, in the light of the results presented here, the impact of reflection-mode X-ray absorption spectroscopy for future experiments should be ensured.

We would like to thank U. Haake, D. Novikov and K. Bruder for their manifold help at the beamlines during the experiments and many exciting discussions. The provision of beam time at the DORIS III storage ring and the financial support of the experiments by HASYLAB are gratefully acknowledged.

References

d'Acapito, F., Castrucci, P., Pinto, N., Gunella, R., de Crescenzi, M. & Davoli, I. (2002). *Surf. Sci.* **518**, 183–191.

d'Acapito, F., Fratoddi, I., d'Amato, R., Russo, M. V., Contini, G., Davoli, I., Mobilio, S. & Polzonetti, G. (2004). *Sensors Actuators B*, **100**, 131–134.

Ankudinov, A. L., Ravel, B., Rehr, J. J. & Conradson, S. D. (1998). *Phys. Rev. B*, **58**, 7565–7576.

Apen, E., Rogers, B. R. & Sellers, J. A. (1998). *J. Vac. Sci. Technol. A*, **16**, 1227–1232.

Barr, T. L. (1994). *Modern Esca.* Boca Raton: CRC Press.

Benzi, F., Davoli, I., Rovezzi, M. & d'Acapito, F. (2008). *Rev. Sci. Instrum.* **79**, 103902.

Boer, D. K. G. de (1996). *Phys. Rev. B*, **53**, 6048–6064.

Boer, D. K. G. de & Leenaers, A. J. G. (1996). *Physica B*, **221**, 18–26.

Born, M. & Wolf, W. (1975). *Principles of Optics*, 5th ed. Oxford: Pergamon.

Borthen, P. & Strehblow, H.-H. (1993). *Thin Solid Films*, **226**, 161–163.

Borthen, P. & Strehblow, H.-H. (1995). *Phys. Rev. B*, **52**, 3017–3019.

Borthen, P. & Strehblow, H.-H. (1997). *J. Phys. IV (France)*, **7**(C2), 187–189.

Bosio, L., Cortes, R., Delichère, P., Froment, M. & Joiret, S. (1988). *Surf. Interface Anal.* **12**, 380–384.

Charnock, J. M., England, K. E. R., Farquhar, M. L. & Vaughan, D. L. (1995). *Physica B*, **208**–**209**, 457–458.

Cheong, S., Bunker, B., Hall, D. C., Snider, G. L. & Barrios, P. J. (2001). *J. Synchrotron Rad.* **8**, 824–826.

Cortes, R., Froment, M., Hugot-LeGoff, A. & Joiret, S. (1990). *Corros. Sci.* **31**, 121–127.

Cross, J. O., Newville, M., Rehr, J. J., Sorensen, L. B., Bouldin, C. E., Watson, G., Gouder, T., Lander, G. H. & Bell, M. I. (1998). *Phys. Rev. B*, **58**, 11215–11225.

Davenport, A. J. & Sansone, M. (1995). *J. Electrochem. Soc.* **142**, 725–730.

Filatova, E., Lukyanov, V., Barchewitz, R., André, J.-M., Idir, M. & Stemmler, P. (1999). *J. Phys. Condens. Matter*, **11,** 3355–3370.

Frankenthal, R. P. (1990). *Corros. Sci.* **31**, 59–68.

Gibson, P. N. & Crabb, T. A. (1995). *Nucl. Instrum. Methods Phys. Res. B*, **97**, 495–498.

Grenier, S., Proietti, M. G., Renevier, H., Gonzalez, L., García, J. M., Gérard, J. M. & García, J. (2001). *J. Synchrotron Rad.* **8**, 536–538.

Heald, S. M., Chen, H. & Tranquada, J. M. (1988). *Phys. Rev. B*, **38**, 1016–1026.

Hecht, D., Borthen, P. & Strehblow, H.-H. (1996). *Surf. Sci.* **365**, 263–277.

Hecht, D., Frahm, R. & Strehblow, H.-H. (1996). *J. Phys. Chem. Lett.* **100**, 10831–10833.

Henke, B. L., Gullikson, E. M. & Davis, J. C. (1993). *Atom. Data Nucl. Data Tables*, **54**, 181–342.

Hóly, V. & Baumbach, T. (1994). *Phys. Rev. B*, **49**, 10668–10676.

Iijima, J., Lim, J.-W., Hong, S.-H., Suzuki, S., Mimura, K. & Isshiki, M. (2006). *Appl. Surf. Sci.* **253**, 2825–2829.

Jiang, D. T. & Crozier, E. D. (1997). *J. Phys. IV (France)*, **7**(C2), 247–249.

Jiang, D. T., Crozier, E. D. & Heinrich, B. (1991). *Phys. Rev. B*, **44**, 6401–6409.

Keil, P., Lützenkirchen-Hecht, D. & Frahm, R. (2005*a*). *Europhys. Lett.* **71**, 77–83.

Keil, P., Lützenkirchen-Hecht, D. & Frahm, R. (2005*b*). *Phys. Scr.* T**115**, 246–248.

Koetter, T. G., Wendrock, H., Schuehrer, H., Wenzel, C. & Wentzig, K. (2000). *Microelectron. Reliab.* **40**, 1295–1299.

Król, A., Sher, C. J. & Kao, Y. H. (1988). *Phys. Rev. B*, **38**, 8579–8592.

Lenglet, M., Kartouni, K., Machefert, J., Claude, J. M., Steinmetz, P., Beauprez, E., Heinrich, J. & Celati, N. (1995). *Mater. Res. Bull.* **30**, 393–403.

Lohrengel, M. M., Schultze, J. W., Speckmann, H.-D. & Strehblow, H.-H. (1987). *Electrochim. Acta*, **33**, 733–742.

Luo, G. M., Mai, Z. H., Hase, T. P. A., Fulthorpe, B. D., Tanner, B. K., Marrows, C. H. & Hickey, B. J. (2001). *Phys. Rev. B*, **64**, 245404.

Lützenkirchen-Hecht, D. & Frahm, R. (2001). *J. Synchrotron Rad.* **8**, 478–480.

Lützenkirchen-Hecht, D. & Frahm, R. (2005). *Physica B*, **357**, 213–217.

Lützenkirchen-Hecht, D. & Frahm, R. (2006). *Surf. Sci.* **600**, 4380–4384.

Lützenkirchen-Hecht, D., Wagemaker, M., Keil, P., van Well, A. A. & Frahm, R. (2003). *Surf. Sci.* **538**, 10–22.

Martens, G. & Rabe, P. (1980). *Phys. Status Solidi A*, **58**, 415–424.

Melendres, C. A., Bowmaker, G. A., Leger, J. M. & Beden, B. J. (1998). *J. Electroanal. Chem.* **449**, 215–218.

Millet, B., Fiaud, C., Hinnen, C. & Sutter, E. M. M. (1995). *Corros. Sci.* **37**, 1903–1918.

Névot, L. & Croce, P. (1980). *Rev. Phys. Appl.* **15**, 761–780.

Palasantzas, G. (1993). *Phys. Rev. B*, **48**, 14472–14478.

Parratt, L. G. (1954). *Phys. Rev.* **95**, 359–369.

Ravel, B. & Newville, M. (2005). *J. Synchrotron Rad.* **12**, 537–541.

Ressler, T. (1998). *J. Synchrotron Rad.* **5**, 118–122.

Schmuki, P., Virtanen, S., Davenport, A. J. & Vitus, C. M. (1996). *J. Electrochem. Soc.* **143**, 3997–4005.

Sinha, S. K., Sirota, E. B., Garoff, S. & Stanley, H. B. (1988). *Phys. Rev. B*, **38**, 2297–2311.

Strehblow, H.-H. & Titze, B. (1980). *Electrochim. Acta*, **25**, 839–850.

Tolan, M. (1999). *X-ray Scattering from Soft Matter Thin Films, Springer Tracts in Modern Physics*, Vol. 148. Berlin: Springer.

Tonnerre, J. M., De Santis, M., Grenier, S., Tolentino, H. C. N., Langlais, V., Bontempi, E., García-Fernández, M. & Staub, U. (2008). *Phys. Rev. Lett.* **100**, 157202.

Wagemaker, M., Lützenkirchen-Hecht, D., van Well, A. A. & Frahm, R. (2004). *J. Phys. Chem. B*, **108**, 12456–12464.

Yang, J. C., Kolasa, D., Gibson, J. M. & Yeadon, M. (1998). *Appl. Phys. Lett.* **73**, 2841–2843.

You, H., Melendres, C. A., Nagy, Z., Maroni, V. A., Yun, W. & Roncon, R. M. (1992). *Phys. Rev. B*, **45**, 11288–11298.

Zheng, S., Hayakawa, S. & Gohshi, Y. (1997). *J. Electron Spectrosc. Relat. Phenom.* **87**, 81–89.